

Projection Onto Convex Sets (POCS) Based Signal Reconstruction Framework with an associated cost function

February 11, 2014

Mohammad Tofghi, Kivanc Kose*, A. Enis Cetin
Dept. of Electrical and Electronic Engineering, Bilkent University, Ankara,
Turkey

*Dermatology Department, Memorial Sloan Kettering Cancer Center, New York,
USA

tofighi@ee.bilkent.edu.tr, *kosek@mskcc.org, cetin@bilkent.edu.tr

Abstract

A new signal processing framework based on the projections onto convex sets (POCS) is developed for solving convex optimization problems. The dimension of the minimization problem is lifted by one and the convex sets corresponding to the epigraph of the cost function are defined. If the cost function is a convex function in R^N the corresponding epigraph set is also a convex set in R^{N+1} . The iterative optimization approach starts with an arbitrary initial estimate in R^{N+1} and orthogonal projections are performed onto epigraph set in a sequential manner at each step of the optimization problem. The method provides globally optimal solutions in total-variation (TV), filtered variation (FV), ℓ_1 , ℓ_1 , and entropic cost functions. New denoising and compressive sensing algorithms using the TV cost function are developed. The new algorithms do not require any of the regularization parameter adjustment. Simulation examples are presented.

1 Introduction

A de-noising method based on a new POCS framework is introduced. In standard POCS approach, only a common point of convex constraint sets is determined. It is shown that it is possible to use a convex cost function in this framework [1–5].

Bregman developed iterative methods based on the so-called Bregman distance to solve convex optimization problems [6]. In Bregman's approach, it is necessary to perform a D-projection (or Bregman projection) at each step of the algorithm and it may not be easy to compute the Bregman distance in general [5, 7, 8].

In this article Bregman's older projections onto convex sets (POCS) framework [9, 10] is used to solve convex optimization problems instead of the Bregman distance approach. In the ordinary POCS approach the goal is simply to find a vector which is in the intersection of convex sets [10–35]. In each step of the iterative algorithm an orthogonal projection is performed onto one of the convex sets. Bregman showed that successive orthogonal projections converge to a vector which is in the intersection of all the convex sets. If the sets do not intersect iterates oscillate between members of the sets [36–38]. Since there is no need to compute the Bregman distance in standard POCS, it found applications to many practical problems.

In our approach the dimension of the signal reconstruction or restoration problem is lifted by one and sets corresponding to a given convex cost function are defined. This approach is graphically illustrated in Fig. 1. If the cost function is a convex function in \mathbb{R}^N the corresponding epigraph set is also a convex set in \mathbb{R}^{N+1} . As a result the convex minimization problem is reduced to finding a specific member (the optimal solution) of the set corresponding to the cost function. As in ordinary POCS approach the new iterative optimization method starts with an arbitrary initial estimate in \mathbb{R}^{N+1} and an orthogonal projection is performed onto one of the sets. After this vector is calculated it is projected onto the other set. This process is continued in a sequential manner at each step of the optimization problem. The method provides globally optimal solutions in total-variation, filtered variation, ℓ_1 , and entropic function based cost functions because they are convex cost functions.

The article is organized as follows. In Section 2, the convex minimization method based on the POCS approach is introduced. In Section 3, a new denoising method based on the convex minimization approach introduced in Section 2, is presented. This new approach uses supporting hyperplanes of the TV function and it does not require a regularization parameter as in other TV based methods. Since it is very easy to perform an orthogonal projection onto a hyperplane this method is computationally implementable for many cost functions without solving any nonlinear equations. In Section 5, we present the simulation results and some denoising examples.

2 Convex Minimization Using The Epigraph set

Let us first consider a convex minimization problem

$$\min_{\mathbf{w} \in \mathbb{R}^N} f(\mathbf{w}), \quad (1)$$

where $f : \mathbb{R}^N \rightarrow \mathbb{R}$ is a convex function. We increase the dimension by one to define the following sets in \mathbb{R}^{N+1} corresponding to the cost function $f(\mathbf{w})$ as follows:

$$C_f = \{\underline{\mathbf{w}} = [\mathbf{w}^T \ y]^T : y \geq f(\mathbf{w})\}, \quad (2)$$

which is the set of $N+1$ dimensional vectors whose $(N+1)^{st}$ component y is greater than $f(\mathbf{w})$. This set C_f is called the epigraph of f . We use bold face letters for N dimensional vectors and underlined bold face letters for $N+1$ dimensional vectors, respectively.

The second set that is related with the cost function $f(\mathbf{w})$ is the level set:

$$C_s = \{\underline{\mathbf{w}} = [\mathbf{w}^T \ y]^T : y \leq \alpha, \ \underline{\mathbf{w}} \in \mathbb{R}^{N+1}\}, \quad (3)$$

where α is a real number. Here it is assumed that $f(\mathbf{w}) \geq \alpha$ for all $f(\mathbf{w}) \in \mathbb{R}$ such that the sets C_f and C_s do not intersect. They are both closed and convex sets in \mathbb{R}^{N+1} . Sets C_f and C_s are graphically illustrated in Fig. 1 in which $\alpha = 0$.

The POCS based minimization algorithm starts with an arbitrary $\underline{\mathbf{w}}_0 = [\mathbf{w}_0^T \ y_0]^T \in \mathbb{R}^{N+1}$. We project $\underline{\mathbf{w}}_0$ onto the set C_s to obtain the first iterate $\underline{\mathbf{w}}_1$ which will be,

$$\underline{\mathbf{w}}_1 = [\mathbf{w}_0^T \ 0]^T, \quad (4)$$

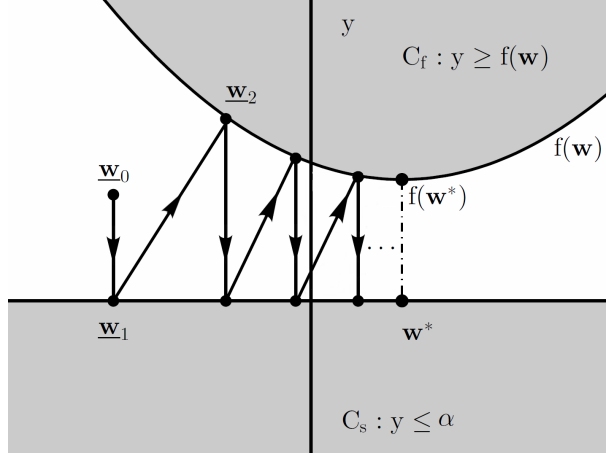


Figure 1: Two convex sets C_f and C_s corresponding to the cost function f . We sequentially project an initial vector $\underline{\mathbf{w}}_0$ onto C_s and CC_f to find the global minimum which is located at \mathbf{w}^* .

where $\alpha = 0$ is assumed as in Fig. 1. Then we project $\underline{\mathbf{w}}_1$ onto the set C_f . The new iterate $\underline{\mathbf{w}}_2$ is determined by minimizing the distance between $\underline{\mathbf{w}}_1$ and C_f , i.e.,

$$\underline{\mathbf{w}}_2 = \arg \min_{\mathbf{w} \in C_s} \|\underline{\mathbf{w}}_1 - \mathbf{w}\|. \quad (5)$$

Equation 5 is the ordinary orthogonal projection operation onto the set $C_f \in \mathbb{R}^{N+1}$. To solve the problem in Eq. 5 we do not need to compute the Bregman's so-called D-projection. After finding $\underline{\mathbf{w}}_2$, we perform the next projection onto the set C_s and obtain $\underline{\mathbf{w}}_3$ etc. Eventually iterates oscillate between two nearest vectors of the two sets C_s and C_f . As a result we obtain

$$\lim_{n \rightarrow \infty} \underline{\mathbf{w}}_{2n} = [\mathbf{w}^* \ f(\mathbf{w}^*)]^T, \quad (6)$$

where \mathbf{w}^* is the N dimensional vector minimizing $f(\mathbf{w})$. The proof of Eq. 6 follows from Bregman's POCS theorem [9, 36]. It was generalized to non-intersection case by Gubin et. al [13, 36], [37]. Since the two closed and convex sets C_s and C_f are closest to each other at the optimal solution case, iterations oscillate between the vectors $[\mathbf{w}^* \ f(\mathbf{w}^*)]^T$ and $[\mathbf{w}^* \ 0]^T$ in R^{N+1} as n tends to infinity. It is possible to increase the speed of convergence by non-orthogonal projections [25].

If the cost function f is not convex and have more than one local minimum then the corresponding set C_f is not convex in R^{N+1} . In this case iterates may converge to one of the local minima.

Consider the standard LASSO based denoising [39]:

$$\min \frac{1}{2} \|\mathbf{v} - \mathbf{w}\|_2^2 + \lambda \|\mathbf{w}\|_1, \quad (7)$$

where \mathbf{v} is the corrupted version of \mathbf{w} . Since the cost function

$$f(\mathbf{w}) = \frac{1}{2} \|\mathbf{y} - \mathbf{w}\|_2^2 + \lambda \|\mathbf{w}\|_1, \quad (8)$$

is a convex function, the framework introduced in this section can solve this problem in an iterative manner. One weakness of this approach is that the smoothing or regularization parameter λ has to be specified or manually selected.

3 De-noising Using POCS

In this section, we present a new method of denoising, based on TV and FV. Let the noisy signal be \mathbf{v} , and the original signal or image be \mathbf{w}_0 . Suppose that the observation model is the additive noise model:

$$\mathbf{v} = \mathbf{w}_0 + \boldsymbol{\eta}, \quad (9)$$

where $\boldsymbol{\eta}$ is the additive noise. In this approach we solve the following problem for denoising:

$$\underline{\mathbf{w}}^* = \arg \min_{\underline{\mathbf{w}} \in C_f} \|\underline{\mathbf{v}} - \underline{\mathbf{w}}\|^2, \quad (10)$$

where, $\underline{\mathbf{v}} = [v^T \ 0]$ and C_f is the epigraph set of TV or FV in R^{N+1} . The TV function which we used for discrete image $\mathbf{w} = [w^{i,j}] \ 0 \leq i, j \leq M-1 \in f : \mathbb{R}^{M \times M}$ is as follows:

$$TV(\mathbf{w}) = \sum_{i,j=1}^M |w^{i+1,j} - w^{i,j}| + \sum_{i,j=1}^M |w^{i,j+1} - w^{i,j}|. \quad (11)$$

The minimization problem is essentially the orthogonal projection onto the set $C_{f,i}$. This means that we select the nearest vector $\underline{\mathbf{w}}^*$ on the set $C_{f,i}$ to $\underline{\mathbf{v}}$. This is graphically illustrated in Fig. 2.

Actually, Combettes and Pesquet and other researchers including us used a similar convex set in denoising and other signal restoration applications []. The following convex set describes all signals whose TV is bounded by ϵ :

$$C_b = \{\mathbf{w} : TV(\mathbf{w}) \leq \epsilon\} \quad (12)$$

The parameter ϵ is a fixed upper bound on the total variation of the signal and it has to be determined in an ad hoc manner a priori. On the other hand we do not specify a prescribed number on the TV in the epigraph approach. The upperbound on TV is automatically determined by the orthogonal projection according to the location of the corrupted signal as shown in Fig. 2.

The denoising solution $\underline{\mathbf{w}}^*$ has the lowest total variation on the line $[\underline{\mathbf{v}}, \underline{\mathbf{w}}^*]$. In current TV based denoising methods [40, 41] the following cost function is used:

$$\min \|\mathbf{v} - \mathbf{w}\|_2^2 + \lambda TV(\mathbf{w}). \quad (13)$$

The solution of this problem can be obtained using the method that we discussed in Section 2. One problem with this approach is the estimation of the regularization parameter λ . One has to determine the λ in an ad hoc manner or by visual inspection. On the other hand we do not require any parameter adjustment in (19).

The denoising solution in (19) can be found by performing successive orthogonal projection onto supporting hyperplanes of the epigraph set C_f . In the first step we calculated $TV(\mathbf{v})$. We also calculate the surface normal at $\underline{\mathbf{v}} = [\mathbf{v}^T \ TV(\mathbf{v})]$ in R^{N+1} and determine the equation of the supporting hyperplane at $[\mathbf{v}^T \ TV(\mathbf{v})]$. We project $\underline{\mathbf{v}} = [\mathbf{v}^T \ 0]$ onto this hyperplane and obtain $\underline{\mathbf{w}}_1$ as our first estimate as shown in Fig. 3. In the second step we project $\underline{\mathbf{w}}_1$ onto the set C_s by simply making its last component zero. We calculate the TV of this vector and the surface normal, and the supporting hyperplane as in the previous step. We project $\underline{\mathbf{v}}$ onto the new supporting hyperplane, etc.

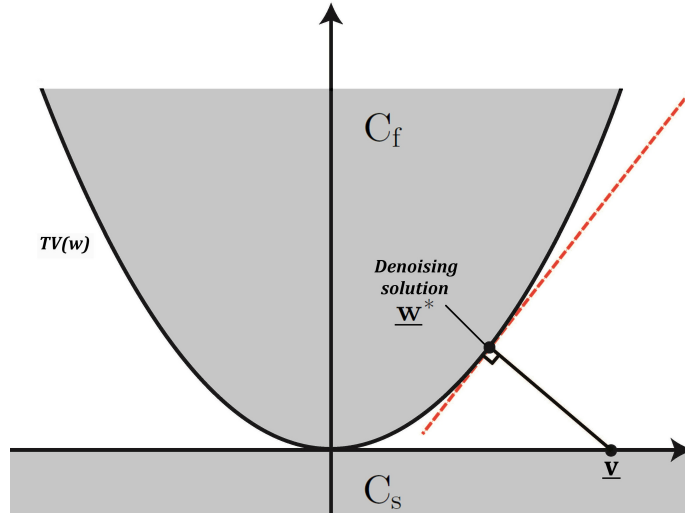


Figure 2: Graphical representation of the minimization of (19). The corrupted observation vector \mathbf{v} is projected onto the set C_f . $TV(\mathbf{w})$ is zero for $\mathbf{w} = [0, 0, \dots, 0]^T$ or when it is a constant vector.

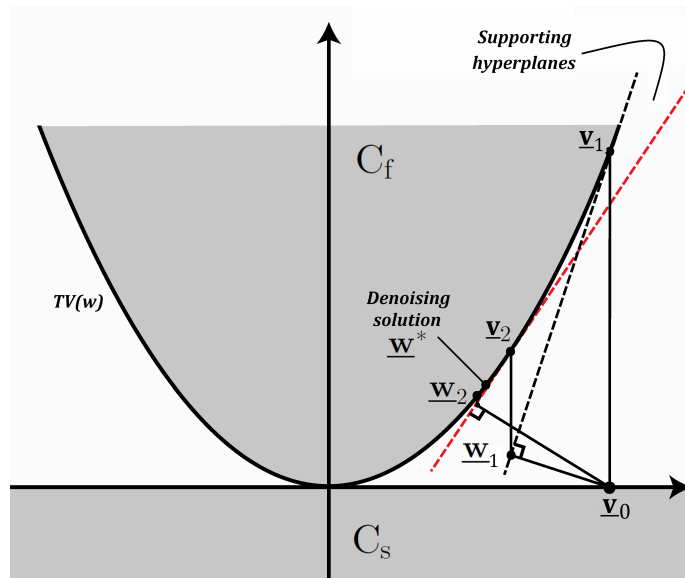


Figure 3: Graphical representation of the minimization of (19), using projection onto the supporting hyperplanes of C_f .

The sequence of iterations obtained in this manner converges to a vector in the intersection of C_s and C_f . In this problem the sets C_s and C_f intersect because $TV(\mathbf{w}) = 0$ for $\mathbf{w} = [0, 0, \dots, 0]^T$ or for a constant vector. However, we do not want to find a trivial constant vector in the intersection of C_s and C_f . We calculate the distance between \mathbf{v} and \mathbf{w}_i at each step of the iterative algorithm described in the previous paragraph. This distance $\|\mathbf{v} - \mathbf{w}_i\|_2^2$ initially decreases and starts increasing as i increases. Once we detect the increase we perform some refinement projections to obtain the solution of the de-noising problem. A typical convergence graph is shown in Fig. 4 for the “note” image.

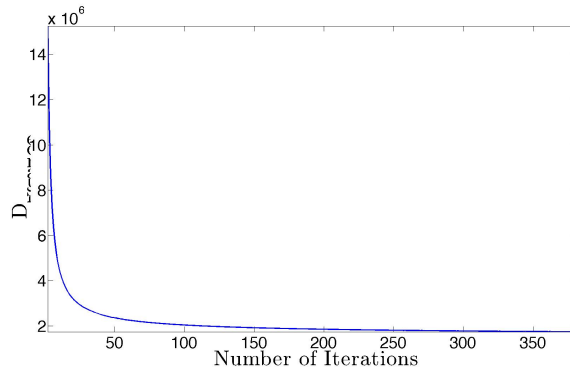


Figure 4: Orthogonal distance from \mathbf{v} to the epigraph of TV in each iteration.

4 Compressive Sensing

The most common method used in compression applications is transform coding. The signal \mathbf{x} is transformed into another domain defined by the transformation matrix $\boldsymbol{\psi}$. The transformation procedure is simply finding the inner product of the signal \mathbf{x} with the rows ψ_i of the transformation matrix $\boldsymbol{\psi}$ represented as follows:

$$s_l = \langle \mathbf{x}, \psi_l \rangle \quad i = 1, 2, \dots, N, \quad (14)$$

where \mathbf{x} is a column vector of size N .

The discrete time signal can be reconstructed from its transform coefficients s_l as follows:

$$\mathbf{x} = \sum_{l=1}^N s_l \cdot \psi_l \quad \text{or} \quad \mathbf{x} = \boldsymbol{\psi} \cdot \mathbf{s}, \quad (15)$$

where \mathbf{s} is a vector containing the transform domain coefficients s_l .

The basic idea in digital waveform coding is that the signal should be approximately reconstructed from only a few of its non-zero transform coefficients. In most cases, including the JPEG image coding standard, the transform matrix $\boldsymbol{\psi}$ is chosen in such a way that the new signal \mathbf{s} is efficiently represented in the transform domain with a small number of coefficients. A signal x is compressible, if it has only a few large amplitude s_l coefficients in the transform domain and the rest of the coefficients are either zeros or negligibly small-valued.

In a compressive sensing framework, the signal is assumed to be K -Sparse in a transformation domain, such as the wavelet domain or the DCT (Discrete Cosine Transform) domain. A signal with length N is K -Sparse if it has at most K non-zero and $(N - K)$ zero coefficients in a transform domain. The case of interest in Compressive Sensing (CS) problems is when $K \ll N$, i.e., sparse in the transform domain.

The CS theory introduced in [2, 42–45] provides answers to the question of reconstructing a signal from its compressed measurement vector \mathbf{v} , which is defined as follows:

$$\mathbf{v} = \boldsymbol{\psi} \mathbf{x} = \boldsymbol{\psi} \cdot \boldsymbol{\phi} \cdot \mathbf{s} = \boldsymbol{\theta} \cdot \mathbf{s}, \quad (16)$$

where $\boldsymbol{\phi}$ is the $M \times N$ measurement matrix and $M \ll N$. The reconstruction of the original signal \mathbf{x} from its compressed measurements \mathbf{y} cannot be achieved by

simple matrix inversion or inverse transformation techniques. A sparse solution can be obtained by solving the following optimization problem:

$$s_p = \arg \min \|s\|_0 \quad \text{such that} \quad \theta.s = y. \quad (17)$$

However, this problem is an NP-complete optimization problem; therefore, its solution can not be found easily. It is also shown in [2, 42–44] that it is possible to construct the ϕ matrix from random numbers, which are i.i.d. Gaussian random variables. In this case, the number of measurements should be chosen as $cK \log(\frac{N}{K}) < M \ll N$ [42], [2]. With this choice of the measurement matrix, the optimization problem (17) can be approximated by ℓ_1 norm minimization as:

$$s_p = \arg \min \|s\|_1 \quad \text{such that} \quad \theta.s = y. \quad (18)$$

Instead of solving the original CS problem in (17) or (18), several researchers developed methods to reformulate those and approximate the solution through these new formulations. For example, in [46], the authors developed a Bayesian framework and solved the CS problem using Relevance Vector Machines (RVM). Some researchers replaced the objective function of the CS optimization in (17), (18) with a new objective function to solve the sparse signal reconstruction problem [47, 48]. One popular approach is replacing ℓ_0 norm with ℓ_p norm, where $p \in (0, 1)$ or even with the mix of two different norms as in [47–50]. However, in these cases, the resulting optimization problems are not convex. Several studies in the literature addressed ℓ_p norm based non-convex optimization problems and applied their results to the sparse signal reconstruction example [51–53]. We use the epigraph of ℓ_1 norm cost function and the TV cost function together with the measurement hyperplanes to solve this problem. Let

$$C_f = \{f(w) \leq y\} \quad (19)$$

where $f(w)$ is the cost function representing the ℓ_1 norm or the TV function, and the measurement hyperplane sets are defined as follows:

$$C_i = \{w.\phi_i = v_i\}, \quad i = 1, 2, \dots, L \quad (20)$$

All of the above sets are closed and convex sets. Therefore it is possible to devise an iterative signal reconstruction algorithm in R^{N+1} by making successive orthogonal projections onto the sets C_s and C_i .

In this case we replace the level set C_s in Section 2 with the measurement hyperplanes. Since the hyperplanes form an undetermined set of equations their intersection $C_{int} = \cap_i C_i$ is highly unlikely to be an empty set but the intersection of hyperplanes C_{int} may not intersect with the epigraph set C_f . This scenario has not been studied in POCS theory to the best of our knowledge [] but it is very similar to the scenario that we discussed in Section 2.

We solve this problem in an iterative manner by performing successive orthogonal projection onto hyperplane corresponding to measurements $v_i = w.\phi_i$ for $i = 1, 2, \dots, N$, followed by an orthogonal projection onto the epigraph set. As we pointed out in the previous paragraph this case has not been studied in the literature. But it is intuitively clear that iterates oscillate between a vector in the intersection of hyperplanes C_{int} and the closest vector of the epigraph set C_f to

the intersection similar to the approach introduced in Section 2. Therefore we essentially obtain a solution to the following problem:

$$\min \|w_f - w_{int}\|_2 \quad (21)$$

where $w_f \in C_f$ and $w_{int} \in C_{int}$.

If the sets C_f and C_{int} intersect the iterates converge to a vector in the $C_{int} \cap C_f$ by Bregman’s POCS theorem.

In our approach its also possible to define a smoothing parameter in both denoising and compressive sensing solutions as well. The epigraph set C_f can be modified as follows:

$$C_{f,\alpha} = \{\underline{\mathbf{w}} : y \geq \alpha TV(\underline{\mathbf{w}})\}. \quad (22)$$

The choice of the parameter $\alpha > 1$ provides smoother solution than usual and $\alpha < 1$ relaxes the smoothing constraint. Its experimentally observed that $\alpha = 1$ usually provides better de-noising results than optimally selected λ values in standard TV denoising in [40]. Simulation examples are presented in the next section.

5 Simulation Results

We present de-noising examples in Section 5.1 and compressive sensing examples in Sensing 5.2.

5.1 De-noising

Consider the “Note” image shown in Fig. 5a. This is corrupted by a zero mean Gaussian noise with $\delta = 45$ in Fig. 5b. The image is restored using our method and Chombolle’s algorithm [40] and the denoised images are shown in Fig. 5c and 5d, respectively. The λ parameter in (13) is manually adjusted to get the best possible results. Our algorithm not only produce a higher SNR, but also a visually better looking image, and this is observable in two other example images in Fig. 7 and 6, both visually and in the sense of SNR value. Solution results for other SNR levels are presented in Table 1. We also corrupted “Note” image with ϵ -contaminated Gaussian noise (“salt-and-pepper noise”). De-noising results are summarized in Table 2.

In Table 3, de-noising results for 10 other images with two different noise levels are presented. In almost all cases our method produces higher SNR results than the de-noising results obtained using [40]. The performance of the reconstruction is measured using the SNR criterion, which is defined as follows

$$SNR = 20 \times \log_{10}\left(\frac{\|x\|_2}{\|x - x_{rec}\|_2}\right), \quad (23)$$

where x is the original signal and x_{rec} is the reconstructed signal.

Moreover, to illustrate the convergence process of the proposed algorithm with “Note” image corrupted with Gaussian noise with standard deviation equal to 25, we calculated the Normalized Root Mean Square Error (*NRMSE*) as:

$$NRMSE(i) = \frac{\|x_i - x\|}{\|x\|}, \quad (24)$$

Table 1: Comparison of The Results For De-noising Algorithms With Gaussian Noise For Note Image (SNRs are in dB)

Noise std	Input SNR	POCS	Chambolle
5	21.12	30.63	29.48
10	15.12	25.93	24.20
15	11.56	22.91	21.05
20	9.06	20.93	18.90
25	7.14	19.27	17.17
30	5.59	17.89	15.78
35	4.21	16.68	14.69
40	3.07	15.90	13.70
45	2.05	15.08	12.78
50	1.12	14.25	12.25

where x_i is the de-noised image in i^{th} step, and x is the original image. As in Fig. 9, the NRMSE is decreasing from -9 dB to -19 dB.

As another experiment to show the convergence behavior, we display the Normalized Total Variation (NTV) as:

$$NTV(i) = \frac{TV(x_i)}{TV(x)}, \quad (25)$$

where x_i and x are the same as the *NRMSE*. As is obvious in Fig. 10, the Normalized TV curve has converged to almost 1, which is demonstrating the successful convergence. As the last measurement of convergence, consider the error value in each step of the iteration; Fig. 11, shows the error value in each step. These three curves shows that the iterations converge to the desired solution roughly around the 100th iteration. The convergence iteration number depends on the noise level, as here for $\delta = 25$ its almost 100.

5.2 Compressive sensing

For the validation and testing of the proposed algorithm, experiments are carried out with one-dimensional (1D) signals, and two-dimensional (2-D) signals, including 30 different images. For 1-D signal, we've done experiments with the cusp signal, which consists of 1024 samples, and is shown in Figure 12. In the DCT domain, the cusp signal can be approximated sparsely. The sparse random signals consisting of 4 and 25 randomly located non-zero samples with random values, are composed of 128 and 256 samples, respectively. In all the experiments, the measurement matrices ϕ are chosen as Gaussian random matrices.

As the first set of experiments, the original cusp signal is reconstructed, with $M = 204$, 717 measurements and, when $M = 24$, 40 measurements are taken from the $S = 5$ random signal with 128 samples. The reconstructed signals using the TV cost functional based algorithm are shown in Figures 13a, and 13b, 6(a), and 6(b). In DCT domain, the cusp signal has 76 coefficients with large magnitude. Therefore, it can be approximated as $S = 76$ sparse signal in the DCT domain.

Table 2: Comparison of The Results For De-noising Algorithms for ϵ -Contamination Noise For Note Image (SNRs are in dB)

ϵ	σ_1	σ_2	Input SNR	POCS	Chambolle
0.9	5	30	14.64	23.44	20.56
0.9	5	40	12.55	21.39	17.60
0.9	5	50	10.75	19.49	15.54
0.9	5	60	9.29	17.61	13.82
0.9	5	70	7.98	16.01	12.57
0.9	5	80	6.89	14.54	11.37
0.9	10	30	12.56	22.88	19.74
0.9	10	40	11.13	21.00	15.30
0.9	10	50	9.85	19.35	12.47
0.9	10	60	8.58	17.87	10.42
0.9	10	70	7.52	16.38	8.76
0.9	10	80	6.46	15.05	7.45
0.95	5	30	16.75	24.52	23.18
0.95	5	40	14.98	22.59	20.44
0.95	5	50	13.41	20.54	18.45
0.95	5	60	12.10	18.72	16.80
0.95	5	70	10.80	17.13	15.34
0.95	5	80	9.76	15.63	14.11
0.95	10	30	13.68	23.79	20.43
0.95	10	40	12.66	22.09	15.35
0.95	10	50	11.71	20.65	12.28
0.95	10	60	10.72	19.10	10.22
0.95	10	70	9.82	17.59	8.66
0.95	10	80	8.92	16.12	7.34

After reconstructing the original cusp signal using the proposed algorithm with $M = 204$, and 717 measurements, we’ve obtained results of 45 and 58 dB, SNR values. In the case of the experiment with random signals, the proposed method reconstructed the original signal with a slight error when using 30 measurement; however, the samples are detected appropriately. Moreover, it is perfectly reconstructed the original signal when using 50 measurements.

In the next set of experiments, we implemented the proposed algorithm in 2-dimension (2D) and applied it to six well known images from the image processing literature and 24 images from the “Kodak True Color images” database [54]. Table 4 represents the SNR values for compressive sensing with two algorithms for these images with two block-size of 32×32 and 64×64 for both algorithms. The images in Kodak dataset are 24 bit per pixel color images. We first transformed all the color images into YUV color space and used the 8 bit per pixel luminance component (Y channel) of the images in our tests. Figure 14 representing the SNR values for some compressive sensing algorithms with eight different percentages of measurements, ranging from 10% up to 80%.

Table 3: Comparison of The Results For De-noising Algorithms With Gaussian Noise For Different Images With std = 30, 50 (SNRs are in dB)

Images	Noise std	Input SNR	POCS	Chambolle
House	30	13.85	27.43	27.13
House	50	9.45	24.20	24.36
Lena	30	12.95	23.63	23.54
Lena	50	8.50	21.46	21.37
Mandrill	30	13.04	19.98	19.64
Mandrill	50	8.61	17.94	17.92
Living room	30	12.65	21.21	20.88
Living room	50	8.20	19.25	19.05
Lake	30	13.44	22.19	21.86
Lake	50	8.97	20.03	19.90
Jet plane	30	15.57	26.28	25.91
Jet plane	50	11.33	23.91	23.54
Peppers	30	12.65	23.57	23.59
Peppers	50	8.20	21.48	21.36
Pirate	30	12.13	21.39	21.30
Pirate	50	7.71	19.37	19.43
Cameraman	30	12.97	24.13	23.67
Cameraman	50	8.55	21.55	21.22
Flower	30	11.84	21.97	20.89
Flower	50	7.42	19.00	18.88
Average	30	13.11	23.18	22.84
Average	50	8.69	20.82	20.70

We compared our results with the block based compressed sensing algorithm given in [55]. Therefore, we divided the image into blocks and reconstructed those blocks individually. Random measurements, which are 30% of the total number of points in images, are used in tests on both the proposed algorithm and Fowler *et.al.*'s method. On average, for 64×64 , and 32×32 blocks, we achieved approximately 1.24 dB, and 0.42 dB higher SNR respectively, compared to the algorithm given in [55], as shown in Table 4.

In the last set of experiments, we compared our reconstruction results with 4 well known CS reconstruction algorithms from the literature; CoSamp [56], ℓ_1 magic [42], Matching Pursuit (MP) [57], and ℓ_p optimization based CS reconstruction [49] algorithms. In comparison to the ℓ_p optimization based CS reconstruction algorithm, we used three different values for p; $p = [0.8, 1, 1.7]$. With $p = 1$, the algorithm solves the problem given in 18, which is the ℓ_1 norm optimization problem.

In this set of experiments, to reconstruct the original signal, we've also implemented the both algorithms with different number of measurements as in previous set of experiments ranging from 10% to 80% of the total number of the samples of the 1D signal. Then, the SNR values are measured between the original signals

Table 4: Comparison of The Results For Compressive Sensing With Fowlers algorithm and Our Algorithm

Image	Fowler	Fowler	POCS	POCS
	B=32	B=64	B=32	B=64
Kodak(ave.)	21.40	21.36	21.96	22.74
Mandrill	16.47	16.77	16.65	16.96
Lena	26.82	26.71	26.02	26.86
Barbara	20.05	20.40	18.21	18.62
Peppers	24.66	24.46	27.06	27.93
Goldhill	22.78	23.44	23.64	24.24
Average	21.60	21.53	22.02	22.77

and the reconstructed ones. The main region of interest in these experiments is 20% – 60% range. The results of the tests with cusp signal are presented in Fig. 14. The proposed algorithm in almost all of the cases performed better than other algorithms. As another measurement of convergence, we calculated the error in each step of the iterations, and as in Fig. 17, the error cure converges almost to zero for $M = 307$ (30% of signal length). It is important to note that, the cusp signal is not sparse; however, since the coefficients in most of the transform domains are not zero, but close to zero, then it is compressible [58]. Therefore, the sparsity level of the test signals are not known exactly beforehand.

6 Conclusion

A new de-noising method based on the epigraph of the TV function is developed. The solution is obtained using POCS. The new algorithm does not need the optimization of the regularization parameter.

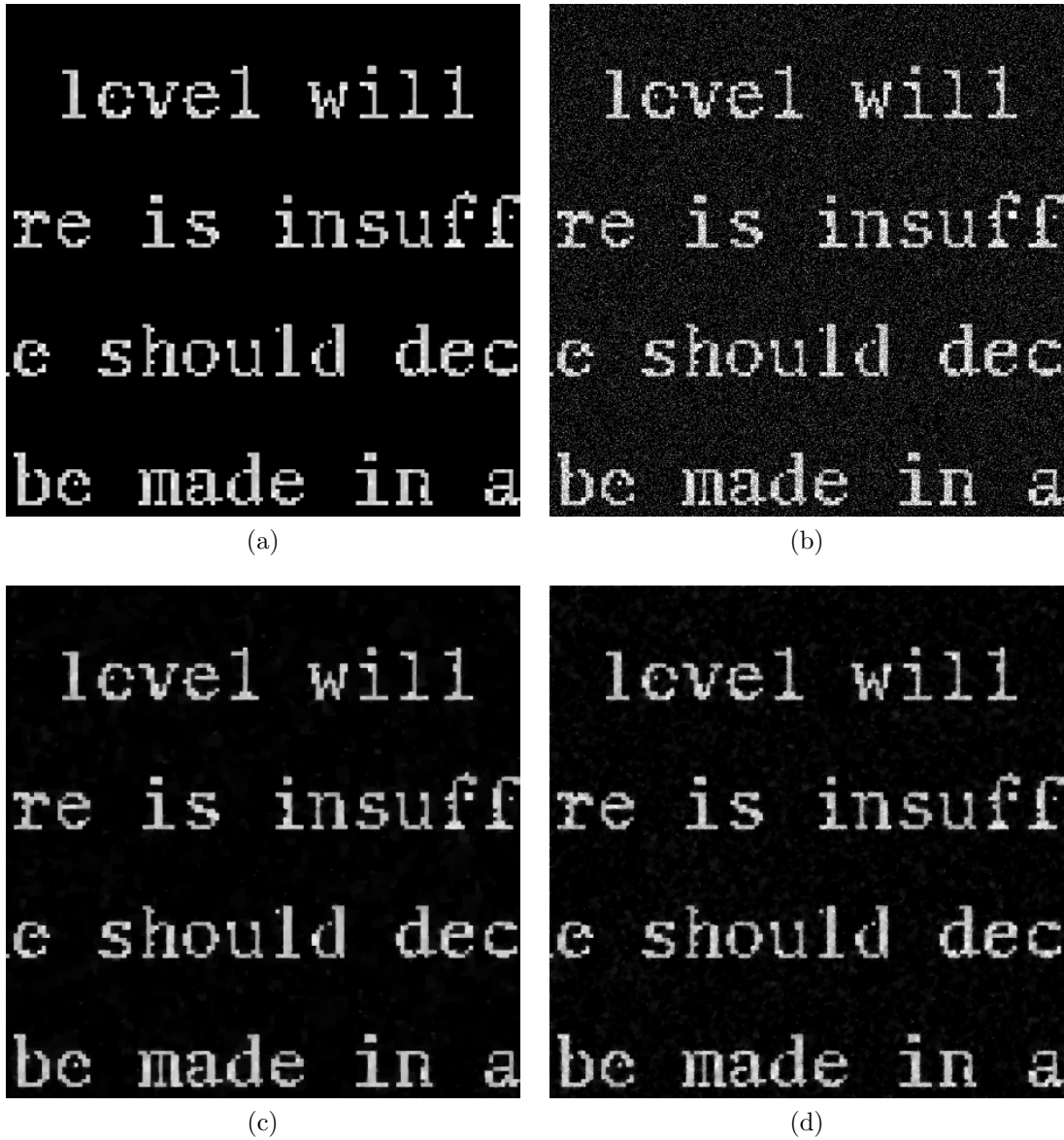
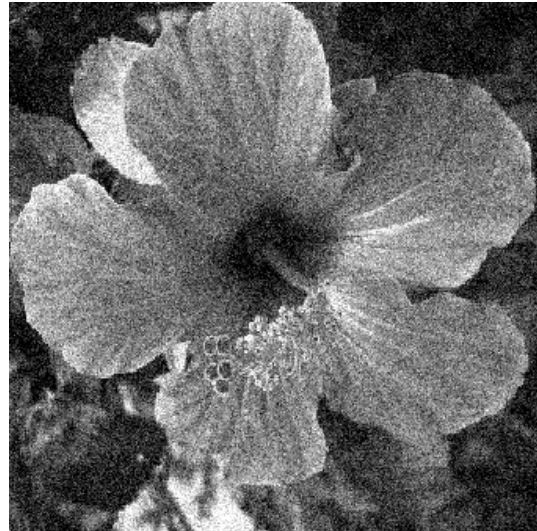


Figure 5: Sample images used in our experiments (a) Original “Note” image, (b) “Note” image corrupted with Gaussian noise with $\delta = 45$, (c) Denoised “Note” image, using POCS algorithm; SNR = 15.08 dB, (d) Denoised “Note” image, using Chambolle’s algorithm; SNR = 12.78 dB.



(a)



(b)



(c)



(d)

Figure 6: Sample images used in our experiments (a) Original “Flower” image, (b) “Flower” image corrupted with Gaussian noise with $\delta = 30$, (c) Denoised “Flower” image, using POCS algorithm; SNR = 21.97 dB, (d) Denoised “Flower” image, using Chambolle’s algorithm; SNR = 20.89 dB.



(a)



(b)



(c)



(d)

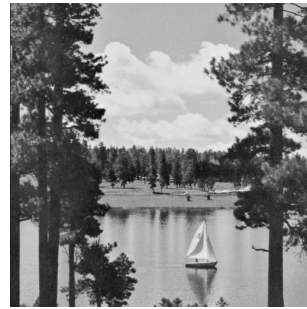
Figure 7: Sample images used in our experiments (a) Original “Cameraman” image, (b) “Cameraman” image corrupted with Gaussian noise with $\delta = 50$, (c) Denoised “Cameraman” image, using POCS algorithm; SNR = 21.55 dB, (d) Denoised “Cameraman” image, using Chambolle’s algorithm; SNR = 21.22 dB.



(a) House



(b) Jet plane



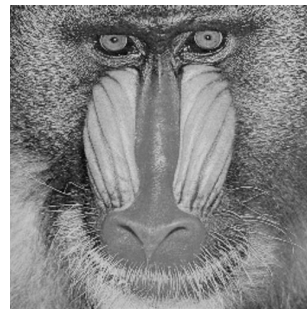
(c) Lake



(d) Lena



(e) Living room



(f) Mandrill



(g) Peppers



(h) Pirate

Figure 8: Sample images used in our experiments (a) House, (b) Jet plane, (c) Lake, (d) Lena, (e) Living room, (f) Mandrill, (g) Peppers, (h) Pirate.

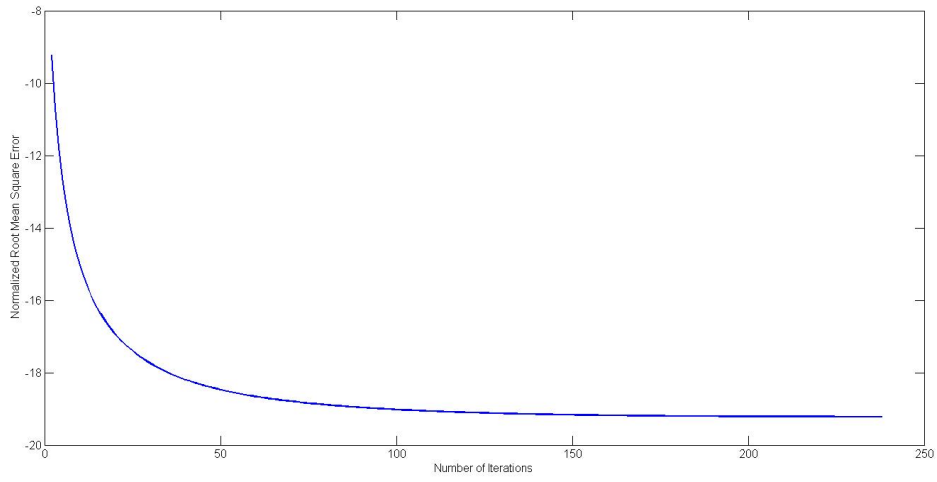


Figure 9: Normalized Root Mean Square Error in each iteration.

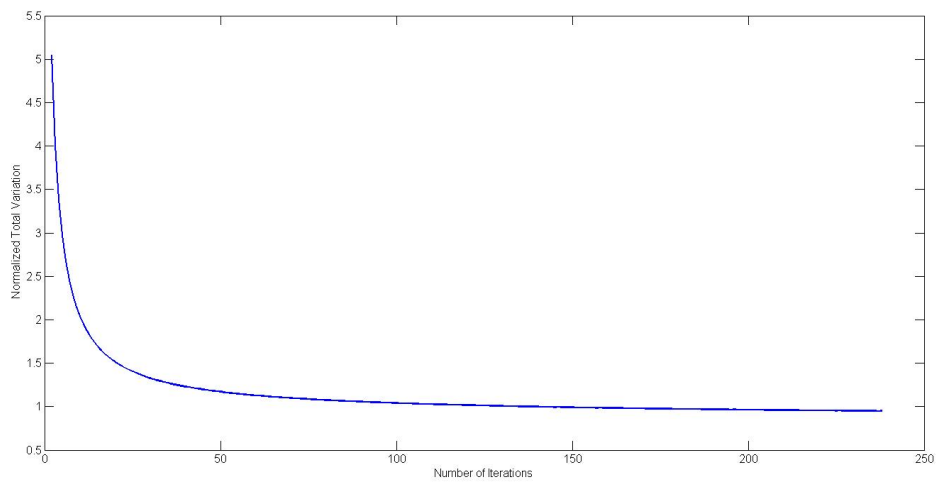


Figure 10: Normalized Total Variation in each iteration.

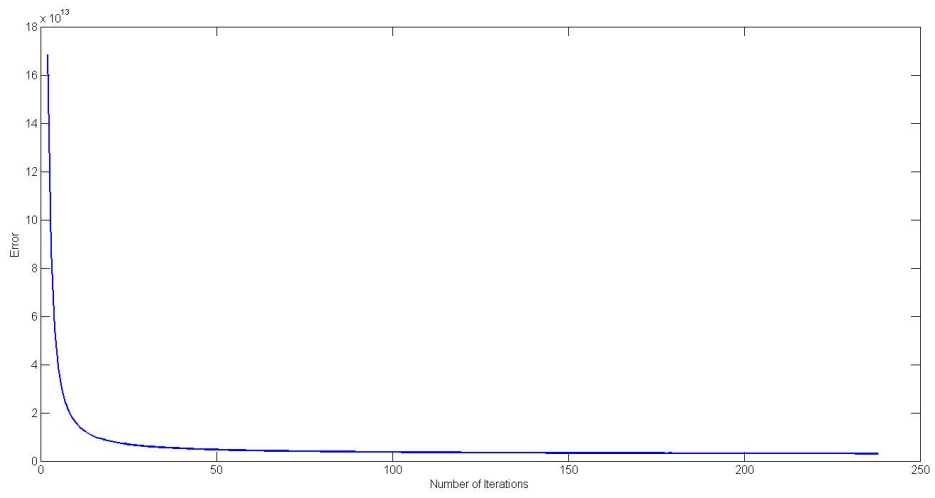


Figure 11: Convergence error curve in each iteration.

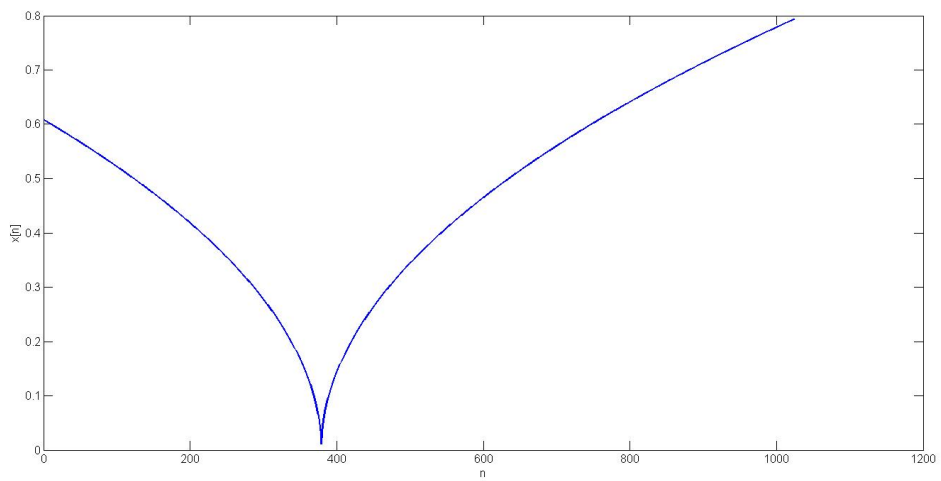
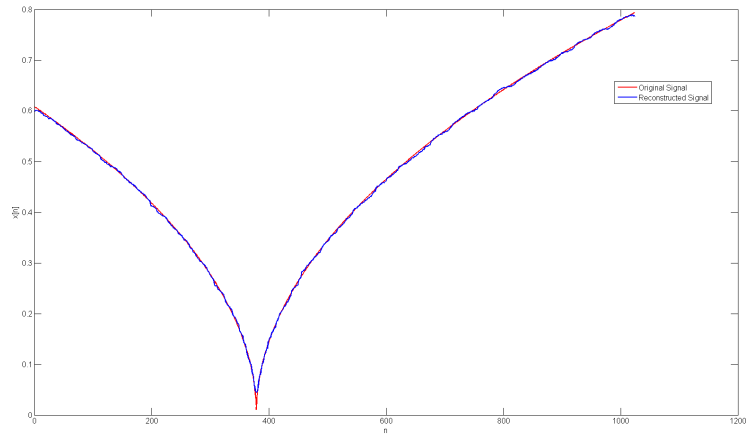
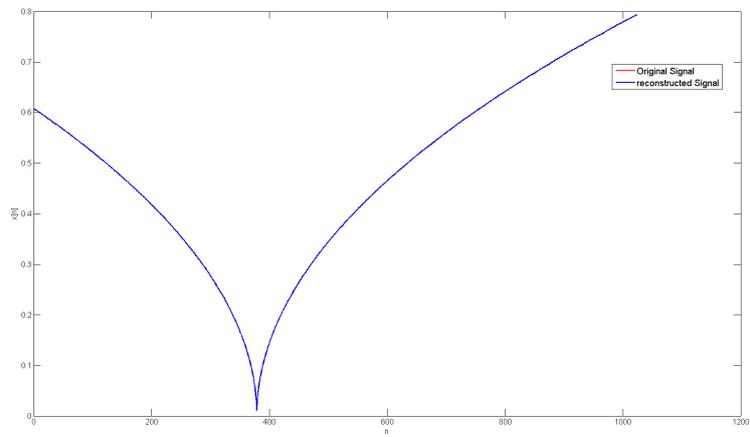


Figure 12: The cusp signal with $N = 1024$ samples.



(a)



(b)

Figure 13: The reconstructed cusp signal with $N = 1024$ samples, for (a) 204 measurements (SNR = 45), and (b) 717 measurements (SNR = 58).

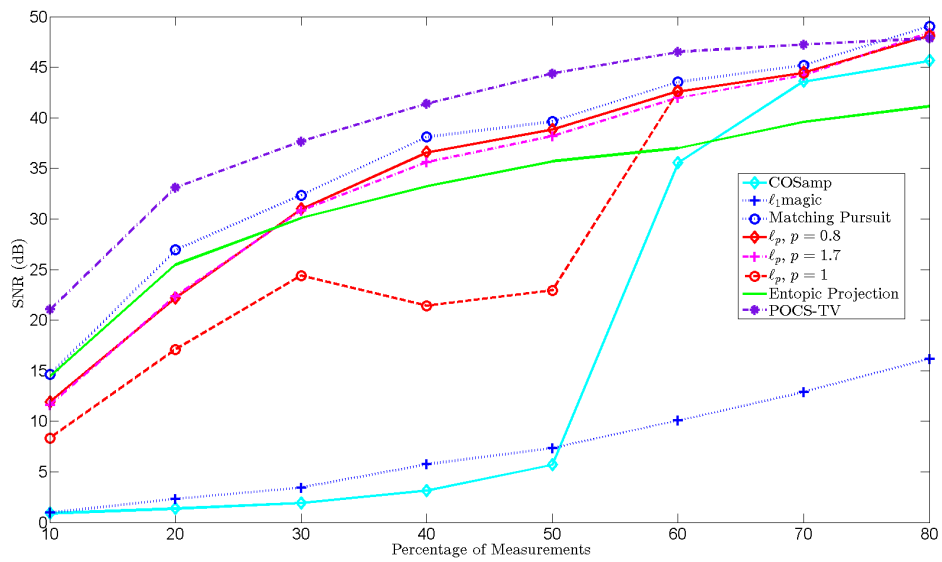


Figure 14: The reconstructed cusp signal with $N = 256$ samples.



(a)



(b)



(c)

Figure 15: Sample results for peppers image with our algorithm (a) Original Image , (b) Reconstructed image with 32x32 blocks, $\text{SNR} = 27.06$, (c) Reconstructed image with 64x64 blocks, $\text{SNR} = 27.93$.



(a)



(b)



(c)

Figure 16: Sample results for peppers image with Fowler's algorithm (a) Original Image , (b) Reconstructed image with 32x32 blocks, SNR = 24.66, (c) Reconstructed image with 64x64 blocks, SNR = 24.46.

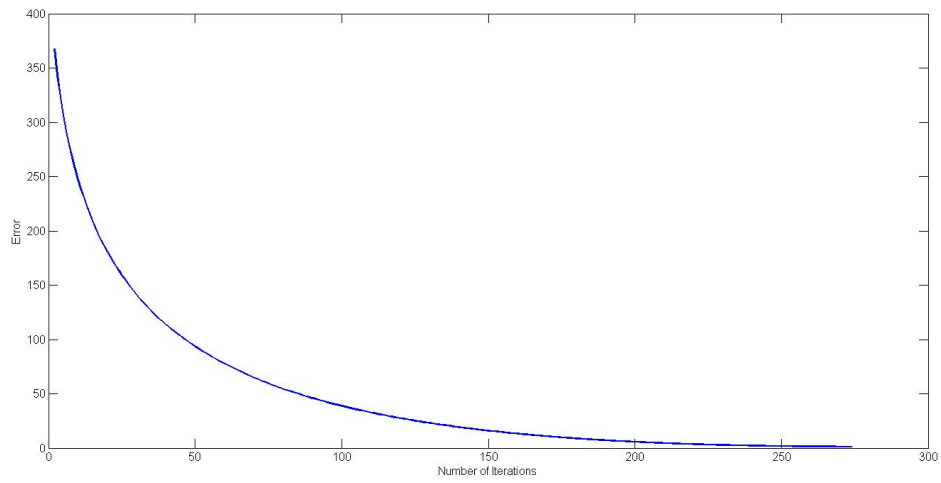


Figure 17: The convergence curve for cusp signal with $N = 1024$ samples, and $M = 307$ measurements.

References

- [1] L. I. Rudin, S. Osher, and E. Fatemi, “Nonlinear total variation based noise removal algorithms,” *Physica D: Nonlinear Phenomena*, vol. 60, no. 1–4, pp. 259 – 268, 1992.
- [2] R. Baraniuk, “Compressive sensing [lecture notes],” *Signal Processing Magazine, IEEE*, vol. 24, no. 4, pp. 118–121, 2007.
- [3] E. Candes and M. Wakin, “An introduction to compressive sampling,” *Signal Processing Magazine, IEEE*, vol. 25, no. 2, pp. 21–30, 2008.
- [4] K. Kose, V. Cevher, and A. Cetin, “Filtered variation method for denoising and sparse signal processing,” *Acoustics, Speech and Signal Processing (ICASSP), 2012 IEEE International Conference on*, pp. 3329–3332, 2012.
- [5] O. Günay, K. Köse, B. U. Töreyn, and A. E. Çetin, “Entropy-functional-based online adaptive decision fusion framework with application to wildfire detection in video,” *IEEE Transactions on Image Processing*, vol. 21, no. 5, pp. 2853–2865, May 2012.
- [6] L. Bregman, “The Relaxation Method of Finding the Common Point of Convex Sets and Its Application to the Solution of Problems in Convex Programming,” *{USSR} Computational Mathematics and Mathematical Physics*, vol. 7, no. 3, pp. 200 – 217, 1967.
- [7] W. Yin, S. Osher, D. Goldfarb, and J. Darbon, “Bregman iterative algorithms for ℓ_1 -minimization with applications to compressed sensing,” *SIAM Journal on Imaging Sciences*, vol. 1, no. 1, pp. 143–168, 2008.
- [8] K. Köse, “Signal and Image Processing Algorithms Using Interval Convex Programming and Sparsity,” Ph.D. dissertation, Bilkent University, 2012.
- [9] L. Bregman, “Finding the common point of convex sets by the method of successive projection.(russian),” *{USSR} Dokl. Akad. Nauk SSSR*, vol. 7, no. 3, pp. 200 – 217, 1965.
- [10] D. Youla and H. Webb, “Image Restoration by the Method of Convex Projections: Part 1 Num2014;theory,” *Medical Imaging, IEEE Transactions on*, vol. 1, no. 2, pp. 81–94, 1982.
- [11] K. Kose, O. Gunay, and A. E. Cetin, “Compressive sensing using the modified entropy functional,” *Digital Signal Processing*, 2013.
- [12] G. T. Herman, “Image Reconstruction from Projections,” *Real-Time Imaging*, vol. 1, no. 1, pp. 3–18, 1995.
- [13] Y. Censor, W. Chen, P. L. Combettes, R. Davidi, and G. Herman, “On the Effectiveness of Projection Methods for Convex Feasibility Problems with Linear Inequality Constraints,” *Computational Optimization and Applications*, vol. 51, no. 3, pp. 1065–1088, 2012.

- [14] K. Slavakis, S. Theodoridis, and I. Yamada, “Online Kernel-Based Classification Using Adaptive Projection Algorithms,” *IEEE Transactions on Signal Processing*, vol. 56, pp. 2781–2796, 2008.
- [15] A. Çetin, H. Özaktas, and H. Ozaktas, “Resolution Enhancement of Low Resolution Wavefields with,” *Electronics Letters*, vol. 39, no. 25, pp. 1808–1810, 2003.
- [16] A. E. Cetin and R. Ansari, “Signal recovery from wavelet transform maxima,” *IEEE Transactions on Signal Processing*, pp. 673–676, 1994.
- [17] A. E. Cetin, “Reconstruction of signals from fourier transform samples,” *Signal Processing*, pp. 129–148, 1989.
- [18] K. Kose and A. E. Cetin, “Low-pass filtering of irregularly sampled signals using a set theoretic framework,” *IEEE Signal Processing Magazine*, pp. 117–121, 2011.
- [19] Y. Censor and A. Lent, “An Iterative Row-Action Method for Interval Convex Programming,” *Journal of Optimization Theory and Applications*, vol. 34, no. 3, pp. 321–353, 1981.
- [20] K. Slavakis, S. Theodoridis, and I. Yamada, “Adaptive constrained learning in reproducing kernel hilbert spaces: the robust beamforming case,” *IEEE Transactions on Signal Processing*, vol. 57, no. 12, pp. 4744–4764, dec 2009.
- [21] K. S. Theodoridis and I. Yamada, “Adaptive learning in a world of projections,” *IEEE Signal Processing Magazine*, vol. 28, no. 1, pp. 97–123, 2011.
- [22] Y. Censor and A. Lent, “Optimization of logx entropy over linear equality constraints,” *SIAM Journal on Control and Optimization*, vol. 25, no. 4, pp. 921–933, 1987.
- [23] H. Trussell and M. R. Civanlar, “The Landweber Iteration and Projection Onto Convex Set,” *IEEE Transactions on Acoustics, Speech and Signal Processing*, vol. 33, no. 6, pp. 1632–1634, 1985.
- [24] P. L. Combettes and J. Pesquet, “Image restoration subject to a total variation constraint,” *IEEE Transactions on Image Processing*, vol. 13, pp. 1213–1222, 2004.
- [25] P. Combettes, “The foundations of set theoretic estimation,” *Proceedings of the IEEE*, vol. 81, no. 2, pp. 182–208, February 1993.
- [26] A. E. Cetin and R. Ansari, “Convolution based framework for signal recovery and applications,” *JOSA-A*, pp. 673–676, 1988.
- [27] I. Yamada, M. Yukawa, and M. Yamagishi, “Minimizing the moreau envelope of nonsmooth convex functions over the fixed point set of certain quasi-nonexpansive mappings,” in *Fixed-Point Algorithms for Inverse Problems in Science and Engineering*. Springer, 2011, pp. 345–390.

- [28] Y. Censor and G. T. Herman, “On some optimization techniques in image reconstruction from projections,” *Applied Numerical Mathematics*, vol. 3, no. 5, pp. 365–391, 1987.
- [29] I. Sezan and H. Stark, “Image restoration by the method of convex projections: Part 2-applications and numerical results,” *IEEE Transactions on Medical Imaging*, vol. 1, no. 2, pp. 95–101, 1982.
- [30] Y. Censor and S. A. Zenios, “Proximal minimization algorithm with d-functions,” *Journal of Optimization Theory and Applications*, vol. 73, no. 3, pp. 451–464, 1992.
- [31] A. Lent and H. Tuy, “An Iterative Method for the Extrapolation of Band-Limited Functions,” *Journal of Mathematical Analysis and Applications*, 83(2), pp.1981, vol. 83, pp. 554–565, 1981.
- [32] Y. Censor, “Row-action methods for huge and sparse systems and their applications,” *SIAM review*, vol. 23, no. 4, pp. 444–466, 1981.
- [33] Y. Censor, A. R. De Pierro, and A. N. Iusem, “Optimization of burg’s entropy over linear constraints,” *Applied Numerical Mathematics*, vol. 7, no. 2, pp. 151–165, 1991.
- [34] M. Rossi, A. M. Haimovich, and Y. C. Eldar, “Conditions for Target Recovery in Spatial Compressive Sensing for MIMO Radar,” 2013.
- [35] R. Baraniuk, V. Cevher, and M. Wakin, “Low-dimensional models for dimensionality reduction and signal recovery: A geometric perspective,” *Proceedings of the IEEE*, vol. 98, no. 6, pp. 959–971, 2010.
- [36] L. Gubin, B. Polyak, and E. Raik, “The Method of Projections for Finding the Common Point of Convex Sets,” *{USSR} Computational Mathematics and Mathematical Physics*, vol. 7, no. 6, pp. 1 – 24, 1967.
- [37] P. L. Combettes, “Algorithmes proximaux pour les problèmes d’optimisation structurés,” 2012.
- [38] A. E. Çetin, O. Gerek, and Y. Yardimci, “Equiripple FIR Filter Design by the FFT Algorithm,” *IEEE Signal Processing Magazine*, vol. 14, no. 2, pp. 60–64, 1997.
- [39] A. Kyrillidis and V. Cevher, “Combinatorial selection and least absolute shrinkage via the clash algorithm,” in *Information Theory Proceedings (ISIT), 2012 IEEE International Symposium on*, 2012, pp. 2216–2220.
- [40] A. Chambolle, “An algorithm for total variation minimization and applications,” *J. Math. Imaging Vis.*, vol. 20, no. 1-2, pp. 89–97, Jan. 2004.
- [41] P. L. Combettes and J.-C. Pesquet, “Proximal splitting methods in signal processing,” in *Fixed-Point Algorithms for Inverse Problems in Science and Engineering*, ser. Springer Optimization and Its Applications, H. H. Bauschke, R. S. Burachik, P. L. Combettes, V. Elser, D. R. Luke, and H. Wolkowicz, Eds. Springer New York, 2011, pp. 185–212.

- [42] E. Candes, J. Romberg, and T. Tao, “Robust uncertainty principles: exact signal reconstruction from highly incomplete frequency information,” *Information Theory, IEEE Transactions on*, vol. 52, no. 2, pp. 489–509, 2006.
- [43] E. J. Candès, “Compressive sampling,” in *Proceedings of the International Congress of Mathematicians*, 2006, pp. 1433–1452.
- [44] E. Candes and T. Tao, “Near-optimal signal recovery from random projections: Universal encoding strategies?” *Information Theory, IEEE Transactions on*, vol. 52, no. 12, pp. 5406–5425, 2006.
- [45] D. Donoho, “Compressed sensing,” *Information Theory, IEEE Transactions on*, vol. 52, no. 4, pp. 1289–1306, 2006.
- [46] S. Ji, Y. Xue, and L. Carin, “Bayesian compressive sensing,” *Signal Processing, IEEE Transactions on*, vol. 56, no. 6, pp. 2346–2356, 2008.
- [47] R. Chartrand, “Exact reconstruction of sparse signals via nonconvex minimization,” *Signal Processing Letters, IEEE*, vol. 14, no. 10, pp. 707–710, 2007.
- [48] T. Rezaii, M. Tinati, and S. Beheshti, “Sparsity aware consistent and high precision variable selection,” *Signal, Image and Video Processing*, pp. 1–12, 2012.
- [49] R. Chartrand and W. Yin, “Iteratively reweighted algorithms for compressive sensing,” in *Acoustics, Speech and Signal Processing, 2008. ICASSP 2008. IEEE International Conference on*, 2008, pp. 3869–3872.
- [50] M. Kowalski and B. Torrèsani, “Sparsity and persistence: mixed norms provide simple signal models with dependent coefficients,” *Signal, Image and Video Processing*, vol. 3, no. 3, pp. 251–264, 2009.
- [51] M. Ehler, “Shrinkage rules for variational minimization problems and applications to analytical ultracentrifugation,” *Journal of Inverse and Ill-posed Problems*, vol. 19, no. 4-5, pp. 593–614, 2011.
- [52] A. Achim, B. Buxton, G. Tzagkarakis, and P. Tsakalides, “Compressive sensing for ultrasound rf echoes using α -stable distributions,” in *Engineering in Medicine and Biology Society (EMBC), 2010 Annual International Conference of the IEEE*, 2010, pp. 4304–4307.
- [53] G. Tzagkarakis and P. Tsakalides, “Greedy sparse reconstruction of non-negative signals using symmetric α -stable distributions,” in *Proceedings of the 18th European Signal Processing Conference (EUSIPCO’10), Denmark*, 2010.
- [54] kodak lossless true color image suite, <http://r0k.us/graphics/kodak/>.
- [55] S. M. J. E. Fowler and E. W. Tramel, “Block-based compressed sensing of images and video,” *Foundations and Trends in Signal Processing*, vol. 4, no. 4, pp. 297–416, 2012.

- [56] D. Needell and J. Tropp, “Cosamp: Iterative signal recovery from incomplete and inaccurate samples,” *Applied and Computational Harmonic Analysis*, vol. 26, no. 3, pp. 301 – 321, 2009. [Online]. Available: <http://www.sciencedirect.com/science/article/pii/S1063520308000638>
- [57] S. Mallat and Z. Zhang, “Matching pursuits with time-frequency dictionaries,” *Signal Processing, IEEE Transactions on*, vol. 41, no. 12, pp. 3397–3415, 1993.
- [58] V. Cevher, M. F. Duarte, C. Hegde, and R. Baraniuk, “Sparse signal recovery using markov random fields,” in *Advances in Neural Information Processing Systems*, 2008, pp. 257–264.